

# ASSESSMENT OF PRISMA ATMOSPHERIC CORRECTION IN HYPERSTROPHIC INLAND WATERS USING 6S AND IN SITU SPECTROSCOPY DATA

Gabriel Rodrigo Caballero<sup>1,2</sup>, Xavier Sòria-Perpinya<sup>1</sup>, Antonio Ruiz-Verdú<sup>1</sup>, Jesús Delegido<sup>1</sup> and José Moreno<sup>1</sup>

<sup>1</sup> Image Processing Laboratory (IPL), University of Valencia, C/Catedrático José Beltrán 2, Paterna, 46980 Valencia, Spain.; gabriel.caballero@uv.es (G.C.); Javier.Soria-Perpina@uv.es (X.S.-P.); antonio.ruiz@uv.es (A.R.-V.); jesus.delegido@uv.es (J.D.); jose.moreno@uv.es (J.M.)

<sup>2</sup> Mantle Labs GmbH, Grünentorgasse 19/4, 1090 Vienna, Austria.; gabriel@mantle-labs.com (G.C.)

## ABSTRACT

The atmospheric correction of hyperspectral remotely sensed images for the retrieval of biogeochemical variables in hypertrophic inland waters is an area of ongoing research. We implemented a radiative transfer model (RTM) processing scheme based on 6S (Second Simulation of the Satellite Signal in the Solar Spectrum) to extrapolate from PRISMA L1 top-of-atmosphere radiance data to above-water remote sensing reflectance (Rrs) in a hypertrophic water reservoir located in Valencia, Spain. We obtained a very good agreement between the in-situ and the atmospherically corrected Rrs ( $R^2 = 0.89$ ,  $RMSE = 0.0017 \text{ sr}^{-1}$ ) within the 400–900 nm wavelength range.

**Key words –** PRISMA, 6S, atmospheric correction, hypertrophic inland waters.

## 1. INTRODUCTION

Hyperspectral remote sensing, characterized by its ability to capture a continuous spectrum of electromagnetic radiation across numerous narrow, contiguous bands, has emerged as a powerful tool for investigating biogeophysical parameters and processes. The past three decades have witnessed a remarkable evolution in Earth Observation (EO) through imaging spectroscopy [1]. The availability of full-spectrum coverage from the visible through near-infrared (VNIR) to the short-wave infrared (SWIR) wavelengths has facilitated the development of standardised validation protocols, robust atmospheric correction methodologies, and innovative retrieval algorithms. These advancements have enabled the derivation of valuable products and applications across terrestrial and aquatic ecosystems.

In recent years, a resurgence of hyperspectral missions has occurred, including DESIS, AHSI, HyperScout-1, HISUI, EnMap and the PRRecursore IperSpettrale della Missione Applicativa (PRISMA) sensor by the Italian Space Agency [2].

To support the Calibration and Validation activities of the PRISMA hyperspectral mission, previous studies have demonstrated the consistency of PRISMA's top-of-atmosphere radiance (LTOA) products with expected values over water targets [3, 4]. In the context of atmospheric correction, radiative transfer models (RTM) offer a convenient tool to accurately simulate the transfer of electromagnetic radiation through the Earth's atmosphere. The RTM 6S (Second Simulation of the Satellite Signal in the

Solar Spectrum) provides an attractive option for estimating atmospheric transmittance, reflectance, and radiance [5]. Furthermore, 6S incorporates a comprehensive representation of atmospheric constituents, including gases, aerosols, and clouds, allowing for realistic simulations under diverse atmospheric conditions.

Building upon this foundation, this research aims to provide an assessment of PRISMA's Level 2D remote sensing reflectance (Rrs) and 6S atmospherically corrected (hereafter 6S-derived) Rrs over a hypertrophic inland water reservoir. The RTM 6S has been used to retrieve the atmospheric parameters necessary to solve the radiative transfer equation and extrapolate from PRISMA L1 TOA radiance to above-water Rrs. The PRISMA Rrs accuracy is evaluated through a meticulous match-up analysis with above-water in-situ Rrs measurements collected by a handheld hyperspectral radiometer.

## 2. MATERIAL AND METHODS

### 2.1. Study site

The study was conducted at the Bellús water reservoir, located in the province of Valencia, Spain (see Figure 1). This reservoir is not only a beloved spot for recreational activities but also a vital water source for the surrounding region. Unfortunately, it has been showing concerning signs of eutrophication, a process characterized by an overabundance of nutrients leading to a decline in water quality. This excessive nutrient enrichment has given rise to issues such as harmful algal blooms and oxygen depletion, posing a threat to the ecosystem and the overall health of the reservoir.

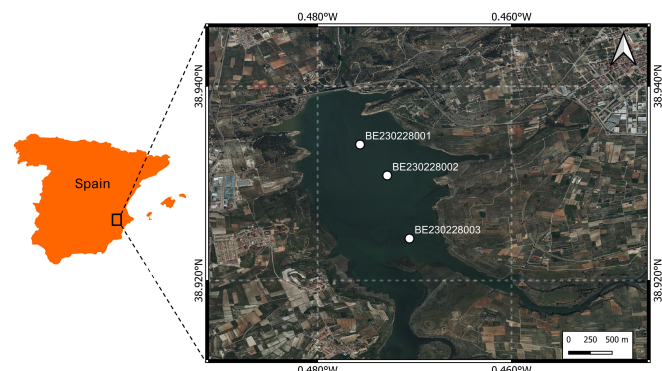


**Figure 1:** Study site: Bellús hypertrophic water reservoir. White dots depicted as BE23022800x show the radiometric sampled point locations. Field campaign conducted on February 28, 2023.

## 2.2. Satellite data and in situ radiometric data

On February 28, 2023, we conducted in-situ measurements of water's Rrs at three different sampling points spread along the Bellús water reservoir. The radiometry data was acquired at 1 nm spectral resolution within the 400–900 nm interval using a portable spectroradiometer (ASD Field Spec®HandHeld 2). The radiometry field campaign was scheduled to coincide with the PRISMA sensor acquisition date, with the sensor passing over the study site at approximately 11:30 a.m. The PRISMA payload is equipped with an advanced hyperspectral sensor comprising both VNIR and SWIR detectors. The sensor has a ground sampling distance of 30 meters and is accompanied by a coregistered 5-meter panchromatic camera. This imaging spectrometer is capable of capturing a hyperdata cube composed of 238 spectral bands ranging from 400 to 2500 nanometers, providing high-quality imaging with a spectral resolution of approximately 12 nanometers [2].

The ground processor systematically produces four different products: PRISMA L1 TOA radiance that is radiometrically corrected and calibrated; Level 2B/C/D geolocated, geocoded atmospherically, and, orthorectified corrected images. The L1 processor converts Level 0 raw imagery from digital numbers to  $L_{TOA}$  expressed in physical radiance units ( $mWm^{-2}sr^{-1}nm^{-1}$ ) using a look-up table (LUT) transfer function. The Level 2 processor transforms the radiance at level L1 TOA into either Bottom-of-Atmosphere (BOA) radiance or reflectance.

## 2.3. Atmospheric correction methodology

In the initial stage of the process, it is assumed that the surface exhibits uniform Lambertian reflectance, meaning that it reflects light equally in all directions. Additionally, it is assumed that the atmosphere is horizontally uniform and varied in composition. Under these assumptions, the quantities measured will be expressed in terms of TOA reflectance, thus  $\rho_{TOA}$  can be defined as:

$$\rho_{TOA} = \frac{L_{TOA} * \pi * d^2}{E_{sun} * \cos(\theta_s)} \quad (1)$$

Where  $L_{TOA}$  is at the sensor-measured radiance,  $E_{sun}$  is the total solar extraterrestrial irradiance at the top of the atmosphere,  $d$  the Sun-Earth distance in astronomical units and  $\theta_s$  is the Sun's zenith angle. To account for the effects of atmospheric gases on PRISMA  $\rho_{TOA}$ , a gas transmittance ( $T_{gas}$ ) correction is applied using either predefined values or user-specified values for atmospheric Ozone ( $O_3$ ) and water vapour ( $H_2O$ ):

$$\rho_{TOA}^* = \frac{\rho_{TOA}}{T_{gas}} \quad (2)$$

Posteriorly, the calculation of  $\rho_{TOA}^*$  is then modelled according to [6]:

$$\rho_{TOA}^* = \rho_{path} + \frac{\rho_s * T^\uparrow * T^\downarrow}{(1 - s_{atm} * \rho_{path})} \quad (3)$$

where  $\rho_{path}$  is the atmospheric path reflectance (combining Rayleigh and aerosols),  $T^\uparrow$  and  $T^\downarrow$  are the total atmospheric

transmittances in the Sun-surface and surface-sensor paths, and  $s_{atm}$  is the spherical Albedo of the atmosphere.

For the atmospheric correction of the PRISMA L1  $L_{TOA}$  the ground surface is considered to be Lambertian, and as the atmospheric conditions are known, the atmospherically corrected reflectance value  $\rho_{s(ac)}$  that will produce the reflectance equal to the TOA reflectance described in Equation 1 entered as input. Following 3,  $\rho_{s(ac)}$  can be determined as:

$$\rho_{s(ac)} = \frac{\rho'_{s(ac)}}{1 + s_{atm} * \rho'_{s(ac)}} \quad (4)$$

with

$$\rho'_{s(ac)} = \frac{\rho_{TOA}^* - \rho_{path}}{T^\uparrow * T^\downarrow} \quad (5)$$

Therefore, the PRISMA atmospherically corrected surface reflectance  $\rho_{s(ac)}$  can be derived from PRISMA  $L_{TOA}$  by combining equations 1, 2, 4, and 5 as shown in the expression below:

$$\rho_{s(ac)} = \frac{(\rho_{TOA}^* - \rho_{path})}{[T^\uparrow * T^\downarrow + s_{atm} * (\rho_{TOA}^* - \rho_{path})]} \quad (6)$$

## 2.4. Atmospheric parameters retrieval and processing workflow

To set up the 6S model, it is important to have the aerosol optical thickness at 550 nm (AOT@550 nm), as well as the  $O_3$  and water vapour levels along the ground-to-sensor path. These atmospheric parameters can be obtained from various freely available catalogues in the Google Earth Engine (GEE) EO database. In the course of this research project, we have incorporated atmospheric data sourced from the following catalogues: NCEP/NCAR Reanalysis Data, for  $H_2O$ , TOMS and OMI Merged Ozone Data for  $O_3$ , and the MOD08 M3.061 Terra Atmosphere Monthly Global Product for AOT@550 nm. The atmospheric correction processing workflow has been fully implemented in Python. We utilized the Py6S package to manage the 6S environment, allowing users to run multiple 6S simulations using a simple Python syntax.

## 2.5. Assesment of atmospheric correction methods

To evaluate the correspondence between PRISMA 2D-level Rrs and 6S-derived Rrs with in-situ measured Rrs, a variety of goodness-of-fit metrics were applied: the coefficient of determination ( $R^2$ ), the root mean square error ( $RMSE$ ), the mean absolute percentage error ( $MAPE$ ), and the  $BIAS$ .

## 3. RESULTS

Figure 2 presents the comprehensive transmittance of the atmosphere ( $T_{gas} * T^\uparrow * T^\downarrow$ ), delineating the distinct contributions of water vapour ( $T_{H_2O}$ ), other gases ( $O_3, O_2, CO_2, CO, NO_2, CH_4$ ), and the combined transmittance resulting from Rayleigh + aerosol effects, both in the upward and downward directions ( $T^\uparrow * T^\downarrow$ ) within the 400–2500 nm wavelength range. These computations

were conducted utilising 6S, in accordance with the PRISMA spectral response functions (SRFs), tailored to the specific geometric parameters of the acquisition day.

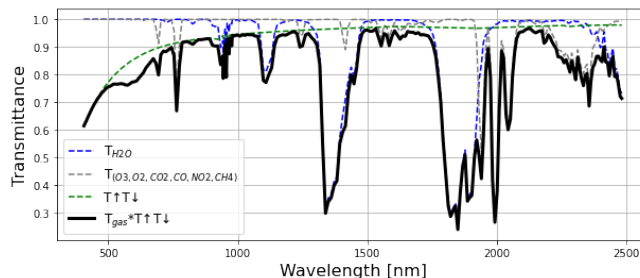


**Figure 2:** Transmittance of the atmosphere simulated with 6S using the atmospheric parameters fetched from GEE for the PRISMA acquisition day and geometry over the study site.

Figure 3 showcases the PRISMA L2D Rrs and the 6S-derived Rrs against the in-situ Rrs for the sampling point BE280323002 (see Figure 1). While surface reflectance data has been successfully obtained for VNIR and SWIR spectral regions, we have deliberately decided to present data within the 400-900 nm wavelength interval. This choice is underpinned by the fact that beyond 900 nm, the water body effectively absorbs most of all incident solar irradiance. This detailed approach allows a more comprehensive understanding of the specific spectral regions where the water's inherent optical properties mainly interact with solar radiation.

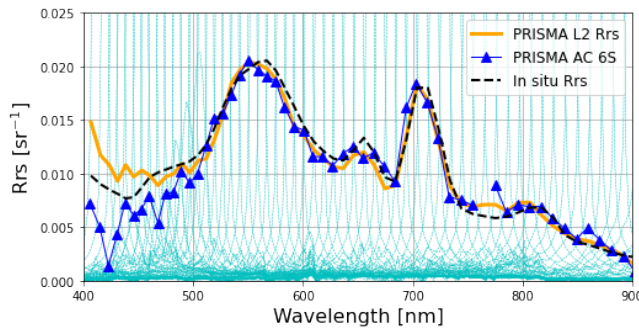


**Figure 3:** PRISMA L2D, 6S-based atmospherically corrected, and in-situ Rrs for a water pixel belonging to Bellús water reservoir. We have only included the Rrs values for the sampling point BE280223002 for simplicity.

In Figure 4, the surface reflectance spectrum of a vegetation pixel located in the proximity of Bellus's basin is depicted across the *VNIR + SWIR* spectral regions. We have specifically excluded the spectral bands that do not meet the requirement  $T_{gas} * T^{\uparrow} * T^{\downarrow} > 0.75$ . The overall transmittance curve is predominantly influenced by the absorbing properties of water vapour, as anticipated in Figure 2.

Table 1 presents the goodness-of-fit metrics values resulting from the comparison of the L2D, 6S-derived, and in-situ Rrs measurements at three hypertrophic water sampling points belonging to Bellús water reservoir. Figure 5 displays the scatter plots depicting the correspondence between the PRISMA L2D and in-situ Rrs and the PRISMA 6S-derived and in-situ Rrs respectively. Lastly, the performance discrepancy between the above water in-situ Rrs measured

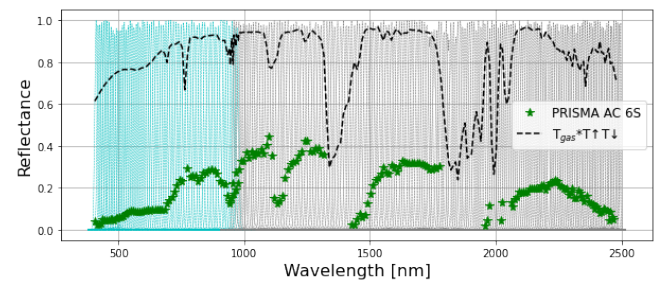


**Figure 4:** Surface reflectance of a vegetation pixel in the vicinity of the study site derived from the PRISMA L1 image atmospherically corrected with 6S RTM.

in the field and the Rrs derived from PRISMA L2D and 6S is displayed in Figure 6.

	R <sup>2</sup>	RMSE	MAPE	Bias	m	b
<b>6S</b>	0.89	0.0017	0.0163	0	0.9517	0.0005
<b>L2D</b>	0.93	0.0013	0.0337	0.0002	0.9229	0.001

**Table 1:** Goodness-of-fit metrics: R<sup>2</sup>, RMSE(sr<sup>-1</sup>), MAPE, Bias (sr<sup>-1</sup>), the slope of the regression line (m) and, the y-intercept (b) for the assesment of the atmospheric correction methods.

#### 4. DISCUSSION

The VNIR spectrum of satellite observations of inland waters is significantly influenced by atmospheric path radiance, accounting for up to 90% of at-sensor radiance. This is primarily caused by atmospheric scattering, with variability due to aerosol concentration and type. Other factors affecting the measurement of Rrs over Bellús inland water reservoir include sun-glint reflectance, high turbidity with non-zero water-leaving radiance in the near-infrared, and the proximity of land (adjacency effects). The statistical analysis presented in Table 1 demonstrates a robust correlation between the PRISMA 6S-derived Rrs and the in-situ Rrs for a hypertrophic water body ( $R^2 = 0.89$ ,  $RMSE = 0.0017$  sr<sup>-1</sup>). In addition, the well-established L2D processor within the PRISMA ground segment consistently delivers highly accurate results ( $R^2 = 0.93$ ,  $RMSE = 0.0013$  sr<sup>-1</sup>) spanning the spectral range of 400 to 900 nm. In the field of imaging spectrometry applied to aquatic environments, it is imperative to recognize the high absorptive nature of these environments. Consequently, their radiometric impact on the at-sensor radiance is relatively minor when juxtaposed with the total radiance detected by the sensor. This phenomenon is particularly pronounced in the blue bands, which experience a substantial contribution from atmospheric path radiance. Figures 3, 5 (bottom), and 5 (top), and 6 show that the 400–500 nm wavelength interval generally yields the weakest correlation results when comparing PRISMA L2D and 6S-derived Rrs against in-situ Rrs as anticipated previously. The signal-to-noise ratio (SNR) poses a notable technical challenge for hyperspectral sensors compared to multispectral sensors. This disparity arises from the inherent trade-off between the narrow bandwidth of the spectral channels and the essential energy required to illuminate detector elements [4]. The SNR of the PRISMA sensor in the VNIR spectral region is particularly lower in the 400–500 nm range

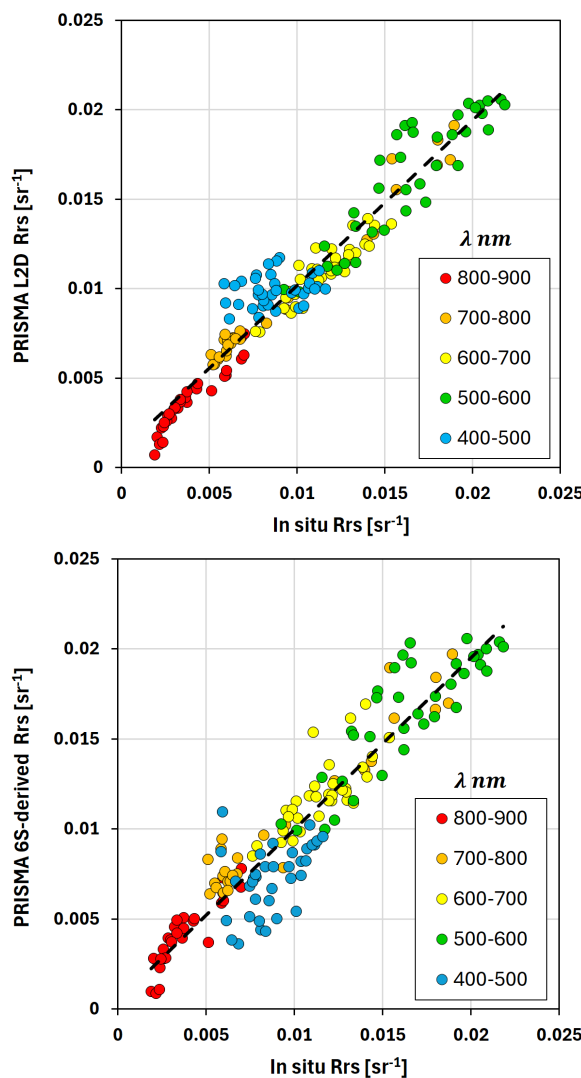


**Figure 5:** The correspondence between PRISMA L2D and in-situ Rrs (top) and between PRISMA 6S-derived and in-situ Rrs (bottom).

due to its radiometric sensitivity. This leads to uncertainties in the atmospheric correction process. There are several factors that can lead to reduced accuracy in Rrs, including the AOT@550 nm,  $O_3$ , and  $H_2O$  estimates obtained from external catalogues available in the GEE EO cloud archive. While using GEE to obtain atmospheric parameters provides flexibility and deployability to our 6S-based atmospheric correction processing workflow, it's important to note that the AOT@550 nm,  $O_3$ , and  $H_2O$  contents should be estimated from the PRISMA L1 image itself. In future implementations, doing so will result in more precise surface reflectance retrieval over inland water.

## 5. CONCLUSIONS

The research conducted has conclusively demonstrated the reliability and precision of a 6S-based atmospheric correction scheme. This correction scheme was implemented to effectively perform atmospheric correction of PRISMA L1 hyperspectral radiance data over a hypertrophic inland water reservoir. The study also showcased the ability of 6S RTM to accurately estimate atmospheric transmittances within the

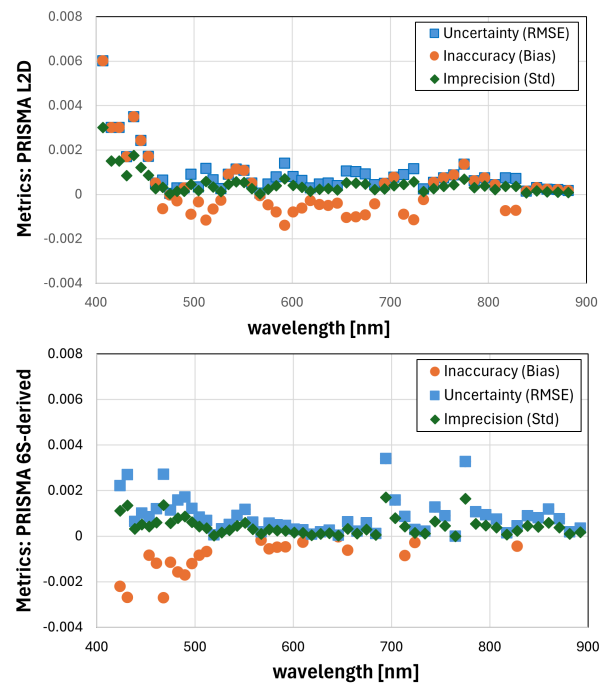


**Figure 6:** Quantification of the lack of performance between PRISMA L2D and in-situ Rrs (top) and between PRISMA 6S-derived and in-situ Rrs (bottom).

400–2500 nm wavelength range.

## 6. REFERENCES

- [1] Alexander F. H. Goetz. Three decades of hyperspectral remote sensing of the Earth: A personal view. *Remote Sens. Environ.*, 113:S5–S16, September 2009.
- [2] S. Cogliati, F. Sarti, L. Chiarantini, M. Cosi, R. Lorusso, E. Lopinto, F. Miglietta, L. Genesio, L. Guanter, A. Damm, S. Pérez-López, D. Scheffler, G. Tagliabue, C. Panigada, U. Rascher, T. P. F. Dowling, C. Giardino, and R. Colombo. The PRISMA imaging spectroscopy mission: overview and first performance analysis. *Remote Sens. Environ.*, 262:112499, September 2021.
- [3] Claudia Giardino, Mariano Bresciani, Federica Braga, Alice Fabbretto, Nicola Ghirardi, Monica Pepe, Marco Gianinetto, Roberto Colombo, Sergio Cogliati, Semhar Ghebrehiwot, Marnix Laanen, Steef Peters, Thomas Schroeder, Javier A. Concha, and Vittorio E. Brando. First Evaluation of PRISMA Level 1 Data for Water Applications. *Sensors (Basel, Switzerland)*, 20(16), August 2020.
- [4] Federica Braga, Alice Fabbretto, Quinten Vanhellemont, Mariano Bresciani, Claudia Giardino, Gian Marco Scarpa, Giorgia Manfè, Javier Alonso Concha, and Vittorio Ernesto Brando. Assessment of PRISMA water reflectance using autonomous hyperspectral radiometry. *ISPRS J. Photogramm. Remote Sens.*, 192:99–114, October 2022.
- [5] Jean-Luc Deuzé. Second Simulation of the Satellite Signal in the Solar Spectrum, 6S: an overview. *IEEE Trans. Geosci. Remote Sens.*, January 1997.
- [6] E. F. Vermote, N. El Saleous, C. O. Justice, Y. J. Kaufman, J. L. Privette, L. Remer, J. C. Roger, and D. Tanré. Atmospheric correction of visible to middle-infrared EOS-MODIS data over land surfaces: Background, operational algorithm and validation. *J. Geophys. Res. Atmos.*, 102(D14):17131–17141, July 1997.